Sequential Monte Carlo Samplers for Semi–Linear Inverse Problems and Application to Magnetoencephalography

Sara Sommariva and Alberto Sorrentino
Dipartimento di Matematica, Genova and CNR–SPIN, Genova

Abstract. We discuss the use of a recent class of sequential Monte Carlo methods for solving inverse problems characterized by a semi–linear structure, i.e. where the data depend linearly on a subset of variables and non–linearly on the remaining ones. In this type of problems, under proper Gaussian assumptions one can marginalize the linear variables. This means that the Monte Carlo procedure needs only to be applied to the non–linear variables, while the linear ones can be treated analytically; as a result, the Monte Carlo variance and/or the computational cost decrease. We use this approach to solve the inverse problem of magnetoencephalography, with a multi–dipole model for the sources. Here, data depend non–linearly on the number of sources and their locations, and depend linearly on their current vectors. The semi–analytic approach enables us to estimate the number of dipoles and their location from a whole time–series, rather than a single time point, while keeping a low computational cost.

1. Introduction

In the Bayesian formulation of inverse problems [27, 24], the unknown and the data are modeled as Random Variables (RVs), and the available information is coded in their probability distributions. When the inverse problem is linear and both the prior density and the likelihood function are Gaussian, the posterior density is also Gaussian, and it is possible to compute analytically standard estimators like the mean and the covariance matrix. On the other hand, characterizing the posterior distribution for non–linear/non–Gaussian problems is typically more difficult, because analytic formulae are seldom available, and one has to resort to numerical approximations, such as Monte Carlo sampling.

In many applied problems, the forward equation establishes a linear dependence of the data on a subset of the unknowns, and a non–linear dependence on the remaining ones. When the likelihood is Gaussian, this entails that the conditional distribution for the linear variables is also normal as long as a Gaussian prior is selected for these variables. In this paper, we discuss how to exploit such linear sub–structure when the posterior distribution is approximated by means of a specific class of Sequential Monte Carlo (SMC) methods, and we apply the method to the inverse source problem in Magnetoencephalography.

Indeed, the term SMC methods is widely used in the literature to refer to a varied class of Monte Carlo algorithms, that include for instance the particle filters [6, 7] for dynamic models. Exploitation of a linear substructure in a particle filter leads to the well–known Rao-Blackwellized particle filter [20, 29]. Importantly, in that case the structure of the equations is such that the distributions over the non-linear variables sampled in the Rao-Blackwellized particle filter are the marginals of those used in the full particle filter.

In the present paper, with the term SMC *samplers* we refer to a specific class of Monte Carlo algorithms, the one described in [4]. These algorithms sample a target distribution, e.g. the posterior of a Bayesian inverse problem, by constructing a sequence of distributions that reaches it smoothly. The underlying idea is the same as that of simulated annealing [14], however, while simulated annealing is a stochastic optimization tool, the SMC samplers approximate the whole posterior distribution. In a couple of recent papers [30, 26] it has been proposed to use Sequential Monte Carlo samplers for solving static inverse problems whose posterior distribution is particularly complex and possibly multimodal. In this paper, we discuss the use of SMC samplers for semi–linear models by means of a *semi–analytic* approach: an SMC sampler is used to approximate only the marginal posterior of the non–linear variables, then the conditional posterior of the linear ones is computed analytically. Similar combinations of analytic calculation and SMC sampler can be found, e.g., in [18] for the case of change point problems, where the model is not semi–linear but still allows exact computation of part of the distribution, and in [9], where the structure of a conditional Hidden Markov Model is exploited analytically with a Kalman smoother.

The first manifest advantage of the semi–analytic approach is that lesser variables are sampled, which expectedly leads to a reduced Monte Carlo variance of the estimators. Perhaps more importantly, this approach becomes particularly interesting when the number of linear variables is relatively high, in that it allows to solve much larger inverse problems than those that can be solved with a *full* SMC, where sampling the full posterior becomes computationally unfeasible. We demonstrate this by applying the method to the inverse problem in magnetoencephalography (MEG). Here the problem is the one to estimate the locations and the current vectors of a small set of sources, whose number is also unknown, given a sampled magnetic field. The data depend non–linearly on the number of sources and on their location, whereas depend linearly on the current vectors. In [26] a full SMC sampler was used to analyze a single topography, i.e. a static spatial distribution of the magnetic field; in the present paper we discuss how to improve this method by exploiting the linear dependence over the current vectors. Moreover MEG data are sampled in time and, since the sampling frequency is usually high, source locations can be assumed to be fixed during a time window up to hundred milliseconds. If one assumes that the number of sources and the source locations are stationary, one can actually apply the semi–analytic approach using a whole time–series to estimate these parameters, thus benefiting from having more signal. As we will show, an additional assumption about the independence of different time points leads

to the pleasant consequence that the computational cost of the proposed method is dominated by calculations that do not depend on the length of the time window. Of course, the same Bayesian model could be approximated, in principle, also with a full SMC; however, the dimension of the state space to be explored with Monte Carlo would increase very quickly, leading to an unbearable computational cost. Alternatively, one could use parametric models for the source time courses, such as those described in [12, 13], at the price of a lower generality of the model.

Another effort towards the estimation of static dipoles from MEG time–series has been done in [25]; however, in that case the problem has been described as a fully dynamic problem, in which also the number of dipoles is allowed to vary in time, and a particle filter was used to approximate dynamically the sequence of posterior distributions. In our model the number of sources is fixed, and the only dynamic variables are the dipole moments, but the computational cost of our new method is definitely lower. On the other hand, exploitation of the linear substructure in the context of multi–dipole models has been performed in [1], where standard Rao–Blackellization was applied to dynamic estimation of dipoles with particle filtering.

The paper is organized as follows. In Sections 2 and 3 we recall the basic ideas behind the use of SMC samplers for Bayesian inverse problems, and specifically for semi–linear inverse problems, respectively. In Section 4 we discuss the application of the semi–analytic method for approximating the posterior distribution for an unknown number of sources in magnetoencephalography, while in Section 5 and 6 we validate it with both synthetic and real MEG data. Finally our conclusions are presented in Section 7.

2. Adaptive Sequential Monte Carlo samplers for Bayesian Inverse Problems

Consider a general Bayesian inverse problem: let Y, X and E be the RVs representing the data, the unknown and the noise, respectively; assume they are related by

$$Y = F(X, E) \tag{1}$$

where F embodies the forward model.

Given a realization of the data $Y = y$, the goal is to approximate the posterior density $\pi(x|y)$, which is related to the prior $\pi(x)$ and to the likelihood function $\pi(y|x)$ by the Bayes' formula

$$\pi(x|y) = \frac{\pi(x)\pi(y|x)}{\pi(y)} \tag{2}$$

where $\pi(y)$ plays the role of the normalizing constant.

Whenever the forward model is non–linear and/or the prior and/or the likelihood are not Gaussian, the resulting posterior distribution tends to be a rather complex

function. In these cases Monte Carlo methods are typically used to characterize such distributions, by providing a sample set that can be used to compute estimators, such as conditional expectations, variance, and so on [24].

In [4] Del Moral et al. presented a particular class of Monte Carlo methods, named Sequential Monte Carlo (SMC) samplers, that result to be particularly good at approximating complex distributions thanks to their sequential nature.
SMC samplers are based on two main ideas:

(i) rather than sampling directly the complex distribution of interest, a one–parameter family of densities is built, that transits *smoothly* from a simpler distribution to the *target* one.
In the case of Bayesian inverse problems, the target distribution is the posterior (2), thus a natural choice for such family is

$$\pi_n(x|y) = \frac{\pi(x)\ \pi(y|x)^{\alpha_n}}{\pi_n(y)} \qquad n = 1, \ldots, N \tag{3}$$

where the likelihood is raised to a tempering exponent that increases with the iterations so that $0 = \alpha_1 < \ldots, < \alpha_N = 1$. As we will describe, the values of these exponents need not to be fixed a priori but can be chosen on-line in a adaptive manner. As observed in [26], such sequence of distributions has a nice interpretation in the case of a Gaussian likelihood: because a Gaussian density raised to an exponent is still a Gaussian density, up to a normalizing factor, each distribution of this sequence can be interpreted as a posterior distribution for a different (decreasing) value of the estimated noise variance.

(ii) since direct importance sampling from this family of distributions is still not applicable, one can actually perform importance sampling in an increasing state space by sampling from a family of artificial joint distributions whose marginals coincide with the original ones. If $\mathcal{X}$ is the state–space for the unknown variable x, one can perform importance sampling on $\mathcal{X}^n = \mathcal{X} \times \cdots \times \mathcal{X}$, defining the target joint distributions

$$\tilde{\pi}_n(x_{1:n}|y) = \pi_n(x_n|y) \prod_{k=2}^{n} L_{k-1}(x_k, x_{k-1}) \tag{4}$$

and the joint importance densities

$$\tilde{\eta}_n(x_{1:n}) = \eta_1(x_1) \prod_{k=2}^{n} K_k(x_{k-1}, x_k) \tag{5}$$

where $x_{1:n} := (x_1, \ldots, x_n)$, while $\{K_k(x_{k-1}, x_k)\}_{k=2}^N$ and $\{L_{k-1}(x_k, x_{k-1})\}_{k=2}^N$ are two families of Markov kernels named forward and backward kernels respectively. The resulting importance weights are naturally defined as

$$w_n(x_{1:n}) = \frac{\tilde{\pi}_n(x_{1:n})}{\tilde{\eta}_n(x_{1:n})} \tag{6}$$

Implementation of these two ideas requires proper choices of the transition kernels involved: in [4] the authors suggest that one can choose $K_k(x_{k-1}, x_k)$ to be a Markov Kernel of invariant distribution $\pi_k(x_k|y)$ and then set

$$L_{k-1}(x_k, x_{k-1}) = \frac{\pi_k(x_{k-1}|y)K_k(x_{k-1}, x_k)}{\pi_k(x_k|y)}, \tag{7}$$

that approximate the *optimal backward Kernels*, i.e. the kernels that minimize the variance of the importance weights [4]. Under these assumptions the algorithm proceeds as follows. An initial set of I weighted particles $\{X_1^i, W_1^i\}_{i=1}^I$ is drawn from the first importance density $\eta_1(x_1)$ usually set equal to the first target distribution $\pi_1(x_1|y) = \pi(x_1)$. Then each particle is let evolve according to the kernels $K_k(x_{k-1}, x_k)$ and the associated unnormalized weight is computed recursively by the formula

$$w_n^i = W_{n-1}^i \pi(y|X_{n-1}^i)^{\alpha_n - \alpha_{n-1}}; \tag{8}$$

then $W_n^i = \frac{w_n^i}{\sum_{j=1}^I w_n^j}$.
Eq. (8) is a consequence of the choice of backward and forward kernels and of the particular choice for the sequence of distributions (3). Moreover it shows that at each iteration the weight associated to the $i-$th particle depends only on the value of the particle at the previous step, and therefore can be calculated before the new particle is drawn. This fact allows to adaptively choose the sequence of tempering exponents for the likelihood in various ways [5, 26, 31]. Here, at each iteration n we compute the normalized weight W_{n+1}^i and the so–called Effective Sample Size (ESS), that is an empirical measure of how much π_{n+1} differs from π_n:

$$ESS(n+1) = \left(\sum_{i=1}^{I} (W_{n+1}^i)^2 \right)^{-1}. \tag{9}$$

Then the increase $\alpha_{n+1} - \alpha_n$ is chosen by a bisection procedure that ends when the ratio $ESS(n+1)/ESS(n)$ falls into a fixed interval. Alternative procedures for this adaptive choice are described e.g. in [31].

It is well–known that in sequential importance sampling the variance of the (unnormalized) importance weights inevitably increases as the iterations proceed; this happens because the weight of most particles tends to become negligible. In other words most computational resources are wasted to explore low–probability regions of the state space. To avoid this phenomenon, said *weight degeneracy*, at each iteration the ESS is computed and if it is lower then a threshold (set to $I/2$ in the simulations below) *systematic resampling* is performed [7], a procedure that consists in removing low–weight particles and replacing them with copies of the high–weight ones: the resampled set, with uniform weights, is an alternative representation of the same distribution.

3. A Semi–Analytic Approach for Conditionally Linear Models

Consider now an inverse problem in which the noise is additive and Gaussian and the forward model has a linear-Gaussian substructure. Our aim is to show how the algorithm presented in the previous section can be modified in order to exploit these structures.

Suppose indeed that the unknown can be split into two sets of variables $X = (R, Q)$ so that

$$Y = G(R)Q + E; \tag{10}$$

observe that the following factorizations for the prior and posterior distributions hold:

$$\pi(x) = \pi(r, q) = \pi(r)\ \pi(q|r) \tag{11}$$

$$\pi(x|y) = \pi(r, q|y) = \pi(r|y)\pi(q|r, y). \tag{12}$$

Moreover suppose that

i) Q, R and E are mutually independent,

ii) $\pi(q|r) = \mathcal{N}(q; \bar{q}_0, \Gamma_{q_0})$,

iii) $\pi_{noise}(e) = \mathcal{N}(e; \bar{e}, \Gamma_e)$,

where $\mathcal{N}(z; m, \Gamma)$ is the Gaussian density of mean m and covariance matrix Γ evaluated in z.

Under these assumptions, for each realization $R = r$ the marginal likelihood $\pi(y|r)$ and the conditional posterior $\pi(q|r, y)$ can be computed analytically. Indeed $\pi(y|r)$ results to be a Gaussian distribution with mean

$$G(r)\bar{q}_0 + \bar{e} \tag{13}$$

and variance

$$G(r)\Gamma_{q_0}G(r)^T + \Gamma_e. \tag{14}$$

Also $\pi(q|y, r)$ is a Gaussian density with mean

$$\bar{q}_0 + \Gamma_{q_0}G(r)^T\Gamma(r)^{-1}(y - G(r)\bar{q}_0 - \bar{e}) \tag{15}$$

and variance

$$\Gamma_{q_0} - \Gamma_{q_0}G(r)^T\Gamma(r)^{-1}G(r)\Gamma_{q_0}, \tag{16}$$

where

$$\Gamma(r) := G(r)\Gamma_{q_0}G(r)^T + \Gamma_e. \tag{17}$$

All these things considered the posterior $\pi(x|y)$ can be approximated through the following two–step algorithm, we refer to as semi–analytic SMC sampler.

First step: we approximate $\pi(r|y)$ through an adaptive SMC sampler.

Reproducing Eq. (3) we sample sequentially from the distributions

$$\pi_n^{SA}(r|y) = \frac{\pi(r)\pi(y|r)^{\alpha_n}}{\pi_n^{SA}(y)} \tag{18}$$

where the sequence of exponents $0 = \alpha_1 < \cdots < \alpha_N = 1$ is chosen adaptively, and the superscript SA is introduced to distinguish these distributions from the marginals of the sequence defined in Eq. (3); the difference between these two sequences will be explained more in detail below.

Second step: for each particle R_N^i obtained at the last iteration of the SMC procedure for $\pi(r|y)$ we analytically compute $\pi(q|R_N^i, y)$ through Eq. (15) and (16).

The main advantage of this method with respect to a SMC sampler procedure applied to approximate the full posterior $\pi(x|y)$ is that only the non–linear variables are sampled while we deal analytically with the linear ones. As we will show by means of simulated experiments this fact leads to some statistical, in terms of a reduction of the Monte Carlo variance of the estimators, and computational improvements.

Remark. As already suggested, the distributions used in the first step of this semi–analytic approach, Eq.(18), are not the marginal distributions of the ones used in the full SMC sampler, Eq.(3).
Indeed marginalizing Eq. (3) we obtain

$$\pi_n(r|y) = \int \pi_n(r, q|y)\ dq = \frac{\pi(r)}{\pi_n(y)} \int \pi(q|r)\pi(y|r, q)^{\alpha_n} dq, \tag{19}$$

while from Eq. (18)

$$\pi_n^{SA}(r|y) = \frac{\pi(r)}{\pi_n^{SA}(y)} \left(\int \pi(q|r)\pi(y|r, q)\ dq \right)^{\alpha_n}. \tag{20}$$

Furthermore under assumption ii) and iii) that ensure a Gaussian distribution for the conditional prior $\pi(q|r)$ and for the likelihood function $\pi(y|r, q)$ we can obtain more explicit expressions that are respectively

$$\pi_n(r|y) = \frac{\pi(r)}{\widehat{\pi_n}(y)}\, \mathcal{N}(y\ ;\ G(r)\bar{q}_0 + \bar{e}\ ,\ G(r)\Gamma_{q_0}G(r)^T + \frac{1}{\alpha_n}\Gamma_e) \tag{21}$$

$$\pi_n^{SA}(r|y) = \frac{\pi(r)\det\left(\Gamma(r)\right)^{\frac{1-\alpha_n}{2}}}{\widehat{\pi_n}^{SA}(y)}\, \mathcal{N}(y\ ;\ G(r)\bar{q}_0 + \bar{e}\ ,\ G(r)\frac{1}{\alpha_n}\Gamma_{q_0}G(r)^T + \frac{1}{\alpha_n}\Gamma_e), \tag{22}$$

where

$$\widehat{\pi_n}(y) = \pi_n(y)\ \alpha_n^{\frac{N}{2}}\ \left[(2\pi)^N\ \det\Gamma_e\right]^{\frac{\alpha_n - 1}{2}} \qquad \widehat{\pi_n}^{SA}(y) = \pi_n^{SA}(y)\ \alpha_n^{\frac{N}{2}}\ (2\pi)^{\frac{N(\alpha_n - 1)}{2}},$$

being N the size of the square matrix Γ_e, are the normalizing constants.

Coherently with the interpretation given in [26], Eq. (21) shows that the distributions $\pi_n(r|y)$ differ from each other only for the noise covariance matrix which is multiplied by $1/\alpha_n$. Instead Eq. (22) shows that the distributions used by the semi–analytic SMC sampler, $\pi_n^{SA}(r|y)$, can be interpreted as the marginals of the posterior distributions of a Bayesian model in which (i) the noise covariance matrix is multiplied by $1/\alpha_n$, (ii) the covariance matrix of the prior for q is also multiplied by $1/\alpha_n$, and (iii) the marginal prior $\pi(r)$ is multiplied by $(\det(\Gamma(r)))^{\frac{1-\alpha_n}{2}}$.

4. Application to Magnetoencephalography

We present here the application of the semi–analytic approach described above to the analysis of magnetoencephalographic data. The present study improves and extends the work presented in [26], where a full SMC sampler was used to approximate the full posterior $\pi(x|y)$. The improvement stems from the fact that the linear variables are marginalized, and therefore are not sampled; as a consequence, it becomes computationally feasible to estimate the non–linear parameters using a whole time–series rather than a single topography.

4.1. The MEG inverse problem

MEG is a non-invasive functional neuroimaging technique that records the weak magnetic field produced by neural currents by means of an helmet–shaped array of SQUID sensors [11]. The physical process that goes from the neural currents to the measured field is modelled by the Biot-Savart equation [21]. From the mathematical point of view, the reconstruction of neural currents from MEG data is an ill-posed problem; indeed the Biot-Savart operator is compact and the solution is not unique [21, 8, 3]. Since MEG data are recorded at a typical frequency of around 1,000 Hertz, estimation of neural currents can benefit from the use of spatio–temporal analysis. In this paper we use a multi–dipole model for the neural currents, i.e. neural currents are represented as the superposition of a small number of point-like currents, termed currents dipoles, each of which models the activity of a small brain area. A current dipole is an applied vector, described by a location and a dipole moment, containing strength and orientation of the current. In this model, it is rather typical to assume that the dipole locations remain fixed for relatively long time intervals, from ten to few hundred milliseconds, as they represent the activity of a given neural population. On the other hand, the dipole moments change in time, as the number of firing neurons and the degree of synchronization between them changes. As we will show, using this model the MEG inverse problem can be formalized by an equation of type (10) and thus the semi–analytic approach can be used.

In order to implement the multi–dipolar approximation, first of all we discretize the brain volume into N_C cells, and for each cell we choose a reference point of position $\mathbf{z}(c)$, $c = 1, \ldots, N_C$. Then neural currents are modeled as the superposition of a small number of current dipoles that are allowed to be located only in the points of the brain grid previously defined:

$$x = \sum_{k=1}^{d} q^{(k)} \delta(\mathbf{z}', \mathbf{z}(c^{(k)})) \tag{23}$$

where $\delta(\cdot, \cdot)$ is the Kronecker delta, d is the number of active dipoles, $c^{(k)} \in \mathbb{N}$, $k = 1, \ldots, d$ are the indices of the grid points where there is a dipole and $q^{(k)} \in \mathbb{R}^3$, $k = 1, \ldots d$ are applied vectors representing the moment of each dipole.

Thus in the framework of multi–dipolar approximation the MEG inverse problem

consists in the estimation of the number of active dipoles, their locations and their time–varying moments from the recorded magnetic field. From the Biot-Savart equation we have that the magnetic field produced by neural currents (23) depends non–linearly on the number of sources and on their locations, and depends linearly on the dipole moments so that we can write

$$\mathbf{y} = \widetilde{G}(r)\mathbf{q} + \mathbf{e} \tag{24}$$

where

- $\mathbf{y} = (y_1, \ldots, y_{N_t})$ is a vector of length $N_s \cdot N_t$, containing the recordings made by the N_s sensors for all the N_t time points;
- $r = (d, c^{(1)}, \cdots, c^{(d)})$ is the collection of the non–linear variables, i.e. the number of sources d and the indices of the source locations in the brain grid $c^{(k)}$;
- $\widetilde{G}(r)$ is the block–diagonal matrix which is obtained as

$$\widetilde{G}(r) = \begin{pmatrix} G(r) & 0 & \cdots & 0 \\ 0 & G(r) & \ddots & \vdots \\ \vdots & \ddots & \ddots & 0 \\ 0 & \cdots & 0 & G(r) \end{pmatrix}. \tag{25}$$

  where $G(r)$ is a matrix of size $(N_s) \times (3 \cdot d)$; each column of $G(r)$ contains the magnetic field produced by a unit dipole, placed in one of the grid points contained in r, and oriented along one of the three orthogonal directions; the number of blocks is equal to the number of time–points, in accordance with the assumption that the number of sources and their locations do not change with time; $\widetilde{G}(r)$ is therefore of size $(N_s \cdot N_t) \times (3 \cdot d \cdot N_t)$;
- $\mathbf{q} = \left(q_1^{(1)}, \ldots, q_1^{(d)}, \ldots, q_{N_t}^{(1)}, \ldots, q_{N_t}^{(d)}\right)$ is a vector of length $3 \cdot d \cdot N_t$, containing the dipole moments of the d dipoles at all N_t time points;
- $\mathbf{e} = (e_1 \ldots, e_{N_t})$ is a vector of length $N_s \cdot N_t$, containing the noise affecting the measurements.

Therefore, under suitable Gaussian assumptions about the noise model and the prior for the dipole moment we can use the semi–analytic approach. As we will show in the next section, the computation can be simplified if we assume the independence between different time points, that means we assume a block–diagonal matrix as the covariance matrix for the Gaussian distribution of noise and prior.

4.2. Statistical model and algorithm settings

In order to apply the semi–analytic approach described in the previous section, we need to define the Bayesian model, i.e. the prior distribution and the likelihood function, and the transition kernels $K_k(r_{k-1}, r_k)$ used for the evolution of the particles in the SMC

procedure.

The parameters of the prior distribution are set in order to reflect neurophysiological knowledge and to satisfy the constraints imposed by the semi–analytic approach. For the distributions over the number of dipoles and their location we follow the same strategy proposed in [26], that we report here in the interest of completeness. The prior density for the dipole moment is taken to be a Gaussian distribution in order to fulfill the requirements of the semi–analytic approach.

$\pi(r, \mathbf{q})$ is decomposed into the product:

$$\begin{aligned}\pi(r, \mathbf{q}) &= \pi(d, c^{(1)}, \ldots, c^{(d)}, q_1^{(1)}, \ldots, q_1^{(d)}, \ldots, q_{N_t}^{(1)}, \ldots, q_{N_t}^{(d)}) \\ &= \pi(d)\pi(c^{(1)}, \ldots, c^{(d)}|d)\pi(q_1^{(1)}, \ldots, q_1^{(d)}, \ldots, q_{N_t}^{(1)}, \ldots, q_{N_t}^{(d)}|d, c^{(1)}, \ldots, c^{(d)}).\end{aligned} \tag{26}$$

where $\pi(d)$ regards the number of dipoles and is chosen to be a Poisson distribution with small parameter; for the dipole position we choose $\pi(c^{(1)}, \ldots, c^{(d)}|d)$ to be a uniform distribution under the constraint that different dipoles must occupy different positions. Finally we assume that $\pi(q_1^{(1)}, \ldots, q_1^{(d)}, \ldots, q_{N_t}^{(1)}, \ldots, q_{N_t}^{(d)}|d, c^{(1)}, \ldots, c^{(d)})$ is a zero–mean Gaussian distribution whose covariance matrix $\Gamma_{\mathbf{q}}$ is block–diagonal

$$\Gamma_{\mathbf{q}} = \begin{pmatrix} \Gamma_{q_1^{(1)}} & 0 & \cdots & 0 \\ 0 & \Gamma_{q_1^{(2)}} & \ddots & \vdots \\ \vdots & \ddots & \ddots & 0 \\ 0 & \cdots & 0 & \Gamma_{q_{N_t}^{(d)}} \end{pmatrix}, \tag{27}$$

where $\Gamma_{q_t^{(k)}}$ is the covariance matrix of the individual dipole, that may contain prior information about the local source orientation. This choice corresponds to treating all the time points independently. In the simulations below, we will be using $\Gamma_{q_t^{(k)}} = \sigma_q^2 \mathbf{I}_{3d}$ and discuss the impact of the choice of σ_q on the results; here $\mathbf{I}_{3d}$ is the identity matrix of order $3d$.

As far as the likelihood function is concerned, we choose a zero–mean Gaussian distribution; again, we assume that we can treat the different time points independently, i.e. that noise has no temporal correlation, so that the covariance matrix $\Gamma_{\mathbf{e}}$ is block–diagonal

$$\Gamma_{\mathbf{e}} = \begin{pmatrix} \Gamma_e & 0 & \cdots & 0 \\ 0 & \Gamma_e & \ddots & \vdots \\ \vdots & \ddots & \ddots & 0 \\ 0 & \cdots & 0 & \Gamma_e \end{pmatrix}, \tag{28}$$

where Γ_e is the spatial covariance matrix; in the simulations below we will be using $\Gamma_e = \sigma_e^2 \mathbf{I}_{N_s}$.

Under these assumptions the marginal likelihood $\pi(\mathbf{y}|r)$ can be written as the product of the marginal likelihoods for single time–points:

$$\pi(\mathbf{y}|r) = \prod_{t=1}^{N_t} \mathcal{N}(y_t; \mathbf{0}, \Gamma_t(r)) \tag{29}$$

where $\Gamma_t(r) = G(r)\Gamma_{q_t}G(r)^T + \Gamma_e$, Γ_{q_t} being the submatrix of $\Gamma_{\mathbf{q}}$ containing the covariance for the d dipoles at a given time point, and each Gaussian is zero–mean because the prior for the dipole moments and the likelihood are zero–mean.

Finally, the conditional posterior $\pi(\mathbf{q}|r, \mathbf{y})$ is a Gaussian density with mean

$$\begin{pmatrix} \Gamma_{q_1}G(r)^T\Gamma_1(r)^{-1}(y_1) \\ \vdots \\ \Gamma_{q_{N_t}}G(r)^T\Gamma_{N_t}(r)^{-1}(y_{N_t}) \end{pmatrix} \tag{30}$$

and variance

$$\begin{pmatrix} \Gamma_{q_1} - \Gamma_{q_1}G(r)^T\Gamma_1(r)^{-1}G(r)\Gamma_{q_1} & 0 & \cdots & 0 \\ 0 & \Gamma_{q_2} - \Gamma_{q_2}G(r)^T\Gamma_2(r)^{-1}G(r)\Gamma_{q_2} & \cdots & 0 \\ \vdots & \vdots & \vdots & \vdots \\ 0 & \cdots & 0 & \Gamma_{q_{N_t}} - \Gamma_{q_{N_t}}G(r)^T\Gamma_{N_t}(r)^{-1}G(r)\Gamma_{q_{N_t}} \end{pmatrix}. \tag{31}$$

Thus the distributions over the dipole moments associated to different instants can be treated separately.

In order to implement the SMC sampler, we have to build the transition kernels $K_k(r_{k-1}, r_k)$ that we assume to be $\pi_k(r_k|y)$ invariant. Because the number of dipoles is unknown, we use a variable dimension model and thus we have to jump between spaces of different dimensions, i.e. the state spaces of sets with different number of dipoles.
As suggested in [26], to do this we split the evolution into two steps. First we treat the evolution of the number of dipoles through a Reversible Jump Metropolis-Hastings [10] that accounts for a possible birth or death move. More specifically the proposal density is built as follows. The birth of a new dipole is proposed with probability $P_{birth} = \frac{1}{3}$ and the location of the new dipole is uniformly drawn from the brain grid points not yet occupied; otherwise the death of a dipole, uniformly drawn from the ones that compose the particle, is proposed with probability $P_{death} = \frac{1}{20}$. If no birth or death are proposed or if the suggested move is rejected the particle doesn't change.
After we deal with the evolution of the location of all the dipoles that compose the particle, even the possibly new ones. The evolution of each dipole is treated separately through a Metropolis-Hastings kernel. The new dipole location is drawn from the grid points within a radius of 1 cm from the old position with probability proportional to a Gaussian centered at the starting point.

We end this Section with a brief description of a computational trick we need in order to implement the SMC procedure for the marginal posterior $\pi(r|\mathbf{y})$. As described

in Section 2, at each iteration n the unnormalized weight associated to the i–th particle is computed through the recursive formula

$$w_{n+1}^i = W_n^i \pi(\mathbf{y}|R_n^i)^{\alpha_{n+1}-\alpha_n} \tag{32}$$

thus the likelihood $\pi(\mathbf{y}|R_n^i)$ has to be evaluated.
If the hypothesis of independence just described holds, $\pi(\mathbf{y}|R_n^i)$ is equal to the product of the marginal likelihood over the N_t instants of the time window.
From a computational point of view that means we have to multiply N_t factors that are lower than 1: this may cause underflow for almost all values of N_t except very low ones. In order to prevent this fact we introduce the log-likehood function and we proceed as follows:

(i) for each particle we compute the logarithm of the unnormalized weight

$$\log(w_{n+1}^i) = \log(W_n^i) + (\alpha_{n+1} - \alpha_n) \sum_{t=1}^{N_t} \log(\pi(y_t|R_n^i)); \tag{33}$$

(ii) then we compute the logarithm of the normalizing constant $C_{norm} := \sum_{i=1}^I w_{n+1}^i$ through the *log-sum-exp formula*

$$\log(C_{norm}) = w + \log(\sum_{i=1}^{I} e^{\log(w_{n+1}^i)-w}) \tag{34}$$

where $w = \max_i\{\log(w_{n+1}^i)\}$;

(iii) finally we compute the logarithm of the normalized weight

$$\log(W_{n+1}^i) = \log(w_{n+1}^i) - \log(C_{norm}) \tag{35}$$

and then, only after we have normalized we calculate the exact value of the weights taking the exponential of Eq. (35).

Observe that the same computational trick can be used to calculate the ESS from the logarithm of the normalized weights $\{W_{n+1}^i\}_{i=1}^I$.

4.3. Point estimation

As described in Section 2, at the end of the SMC procedure for $\pi(r|\mathbf{y})$ we obtain a Monte Carlo approximation for the posterior itself through the weighted particles $\{R^i, W^i\}_{i=1}^I$, where the index N of the iteration is henceforward omitted for simplicity of notation. From this approximation, point estimates for the number of active dipoles and their location can be obtained as described in [26]; then a point estimate for the dipole moments over time can be straightforwardly computed from the analytical expression of the conditional posterior $\pi(\mathbf{q}|r, \mathbf{y})$. More specifically, the estimated number of sources

$\widehat{D}$ is defined as the mode of the marginal distribution of the number of dipoles that can be calculated as

$$\mathbb{P}(D = d|\mathbf{y}) = \sum_{i=1}^{I} W^i \delta(d, D^i) \tag{36}$$

where D^i is the number of dipoles of the $i-$th particle R^i.

The estimated locations of the $\widehat{D}$ active sources are the $\widehat{D}$ highest local modes of the intensity measure for the source location conditioned on the estimated number of sources, that can be computed as

$$\mathbb{P}(c|\mathbf{y}, \widehat{D}) = \sum_{i=1}^{I} W^i \delta(\widehat{D}, D^i) \sum_{k=1}^{D^i} \delta(c, C^{(k),i}) \tag{37}$$

where c is a point of the brain grid and $C^{(k),i}$, $k = 1, \ldots, D^i$, is the location of the k–th dipole into the i–th particle. Observe that only the particles with the correct number of dipoles contribute to this measure.

Finally, an estimate of the time–varying dipole moments $\left(\widehat{Q}_1^{(1)}, \ldots \widehat{Q}_1^{(\widehat{D})}, \ldots \widehat{Q}_{N_t}^{(1)}, \ldots \widehat{Q}_{N_t}^{(\widehat{D})}\right)$ is obtained analytically, as the mean of the conditional distribution

$$\pi(q_1^{(1)}, \ldots, q_1^{(\widehat{D})}, \ldots, q_{N_t}^{(1)}, \ldots, q_{N_t}^{(\widehat{D})}|\mathbf{y}, \widehat{D}, \widehat{C}^{(1)}, \ldots \widehat{C}^{(\widehat{D})}) \tag{38}$$

that, in accordance with the results proved in the previous sections, is a Gaussian density.

5. Simulation Experiments

In this section simulated data are used to validate and assess the performance of the semi–analytic approach. More specifically in Section 5.1 we use a large number of datasets to investigate the behaviour of the algorithm under various experimental conditions, as well as the impact of a partially wrong prior. In Section 5.2 a comparison between our approach and the full SMC presented in [26] is made in terms of the Monte Carlo variance of the approximation obtained. Finally in Section 5.3 we present some computational considerations about the computational cost of the algorithm.

5.1. Experiment 1: Validation of the Method

Following [25, 26] we quantify the performances of the method by calculating discrepancy measures between the true and the estimated source configuration. Let $(D, C^{(1:D)}, Q_1^{(1:D)}, \ldots, Q_{N_t}^{(1:D)})$ and $(\widehat{D}, \widehat{C}^{(1:\hat{D})}, \widehat{Q}_1^{(1:\hat{D})}, \ldots, \widehat{Q}_{N_t}^{(1:\hat{D})})$ be the true and the estimated dipole configuration, respectively; we use:

- Δ_d which is the difference between the true and the estimated number of dipoles $\Delta_d = \widehat{D} - D$;

- Δ_c that quantifies the localization error and is defined as

$$\Delta_c = \begin{cases} \min_{\lambda \in \Lambda_{\widehat{D},D}} \frac{1}{\widehat{D}} \sum_{k=1}^{\widehat{D}} \mid \mathbf{z}(C^{(k)}) - \mathbf{z}(\widehat{C}^{(\lambda(k))}) \mid \text{ if } D \geq \widehat{D} \\ \min_{\lambda \in \Lambda_{D,\widehat{D}}} \frac{1}{D} \sum_{k=1}^{D} \mid \mathbf{z}(C^{(\lambda(k))}) - \mathbf{z}(\widehat{C}^{(k)}) \mid \text{ if } D < \widehat{D} \end{cases} , \tag{39}$$

  where $\Lambda_{k,l}$ is the set of all the permutations of k elements drawn from l elements. Δ_c is a modified version of the OSPA metric with no penalty for cardinality errors, which are evaluated separately by Δ_d above. For more details see [22].

In addition, we compare the true and the estimated time courses, i.e. the norm of the dipole moment as a function of time.

In a first series of tests we generated 300 datasets, each one made of 30 time points and containing 2, 3 or 4 sources. For each data set, dipole locations are uniformly drawn from the brain grid points with a reciprocal distance of at least 1 cm. Dipole orientations are uniformly drawn from the unit sphere and do not change in time. In half datasets the source time courses are independent: dipoles are active one after the other, with almost negligible temporal overlap; in the other 150 datasets, the sources have exactly the same time course. In the MEG literature this last condition is usually defined as sources being perfectly *correlated*; while such condition often happens in real scenarios, many well–known inverse methods, such as MUSIC [17, 16] and beamformers [28, 23], encounter difficulties in estimating perfectly correlated sources. In conclusion, in this first experiment the datasets are divided in six groups, according to the number of sources and their temporal correlation.

Synthetically generated data were then perturbed with white Gaussian noise of fixed standard deviation; because the source location and orientation are random, the actual signal–to–noise (SNR) ratio varies considerably for different sources. As an example Figure 1 shows two synthetic MEG times series, both generated by 3 uncorrelated dipoles but with different SNR.

We analyze the 300 data sets setting $I = 1000$, that is a good compromise between the quality of the results and the computational cost; the value σ_e in the likelihood is set equal to the standard deviation of noise, while the parameter σ_{q_0} for the prior over the dipole moment is set equal to 1, according to the dipole strength we have simulated.

Table 1 shows the values of the discrepancy measures Δ_d and Δ_c averaged over runs together with their standard deviations. Figure 2 shows the true and the estimated source time courses, again averaged over runs.

There seem to be a very small difference between the correlated and the uncorrelated case, as far as the estimation of the number of dipoles and of the dipole locations are concerned: the discrepancy measures are slightly higher for the correlated case, where the number of dipoles is under–estimated more (Δ_d is lower then zero) and the average localization error is slightly higher. These two things are of course related: when two sources are very close to each other, it sometimes happens that the algorithm estimates a single source in between, thus contributing to increasing both discrepancies. On the

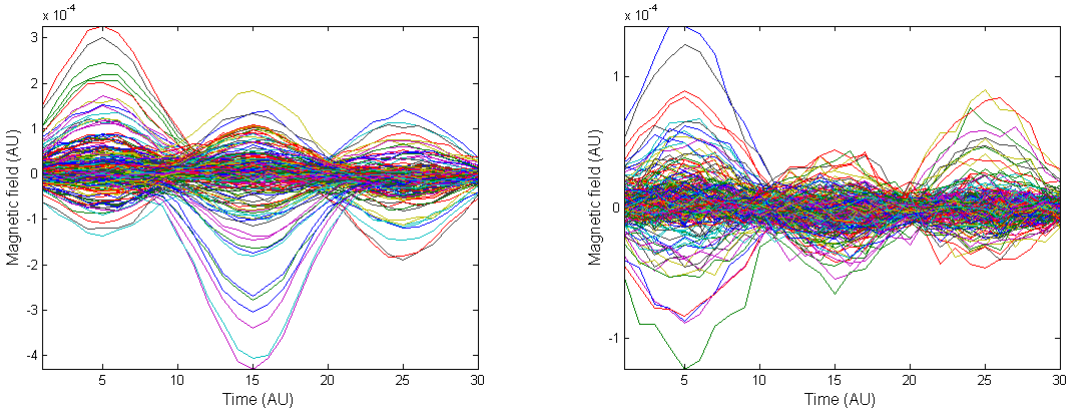

(a) High SNR (b) Low SNR

Figure 1. Two synthetic MEG time–series generated by 3 uncorrelated dipoles. While all the datasets have been perturbed with noise of the same standard deviation, the resulting signal–to–noise ratio varies considerably due to the different locations and orientations of the sources, that produce signals of different intensities.

Unc.	Δ_d	Δ_c
2 dip	0.00 ± 0.00	(0.3 ± 1.1) mm
3 dip	-0.04 ± 0.19	(0.9 ± 1.9) mm
4 dip	-0.04 ± 0.20	(1.0 ± 2.0) mm

Corr.	Δ_d	Δ_c
2 dip	0.00 ± 0.00	(0.7 ± 2.6) mm
3 dip	-0.08 ± 0.27	(1.0 ± 2.6) mm
4 dip	-0.12 ± 0.33	(1.1 ± 1.9) mm

Table 1. Discrepancy measures for the number of dipoles (left) and their location (right) averaged over 50 runs for different numbers of active sources and different levels of correlation.

other hand, both discrepancy measures Δ_d and Δ_r tend to increase with the number of dipoles. This is of course expected, because, as the number of dipoles increases: (i) the ill–posedeness of the problem gets worse, i.e. there may be more alternative configurations explaining the data equally well; (ii) the state–space to be explored increases dramatically, and therefore it becomes more likely to miss the high–probability region; (iii) given the random generation of the data, it becomes more likely that two sources happen to be in nearby locations, and can therefore be explained by a single source. Indeed, a similar behaviour was also observed in [26].

Figure 2 conveys additional information about the proposed method. First, we observe that when the true source strength is zero, the estimated source strength is not (on average). This is in fact a well known pitfall of multi–dipole models with a fixed number of sources: in the temporal window where an estimated source is not actually active, its estimated strength is tuned to optimally explain the noise component in the data. On the other hand, in the case of correlated dipoles the source strengths appear to be slightly over–estimated also at the peak. Going through the datasets one by one, we have observed that this is not a systematic over–estimation, but rather the consequence of occasional and diverse estimation errors in a few datasets: in two two–dipole cases,

the estimated source locations were deeper than the true ones, thus requiring stronger dipoles to reproduce the measured field; in a couple of three–dipole and four–dipole cases, under–estimation of the number of sources, due to the proximity of two dipoles, led to over–estimation of the strength.

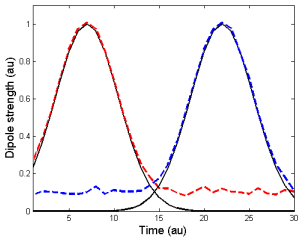

(a) 2 uncorrelated dipoles

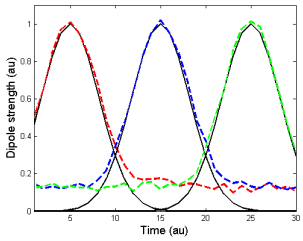

(b) 3 uncorrelated dipoles

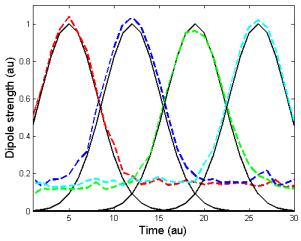

(c) 4 uncorrelated dipoles

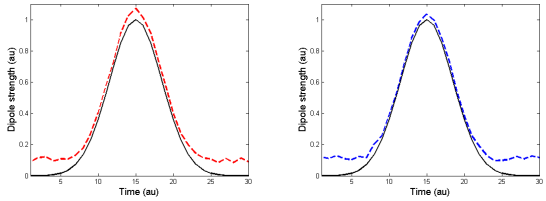

(d) 2 correlated dipoles

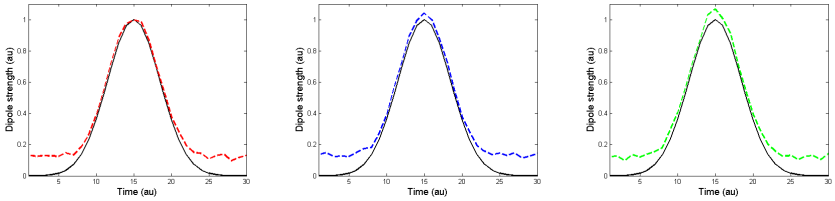

(e) 3 correlated dipoles

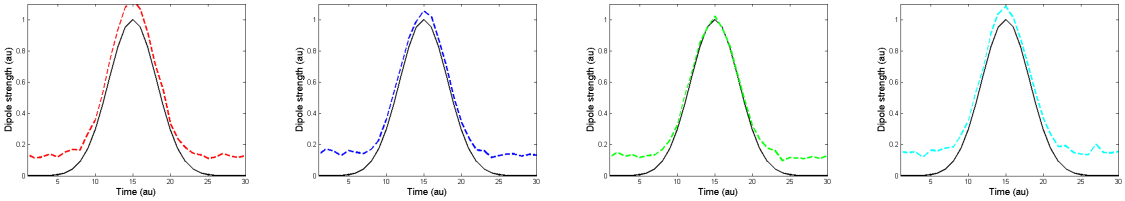

(f) 4 correlated dipoles

Figure 2. Reconstructed dipole strength, $\|Q_t^{(k)}\|$, averaged over runs (dotted lines) superimposed on the true ones (black solid line).

In a second series of tests, we investigated what is the effect of a mis–specification of the prior distribution; namely, we wanted to investigate the robustness with respect to the parameter σ_q, that is the standard deviation of the prior for the dipole moment. To do this, we produced 100 data sets, each one generated by two dipoles of random location; the first dipole has a peak strength of 1, the second dipole has a peak strength of 10; we then applied the algorithm with three different values of σ_q: 1, 5 and 10.

In Table 2 we report the discrepancy measures averaged over these 100 datasets. The results indicate that a mis–specification of the prior can lead to the following cases. When the standard deviation of the prior is 5 or 10, the number of dipoles tends to be under–estimated, because it becomes more likely to miss the weak source. When the standard deviation of the prior is 1, on the other hand, the number of sources tends to be over–estimated, because it sometimes happens that the strong dipole is replaced by two close–by dipoles, whose strengths summing up to 10 (the strength of the true source). While relatively unpleasant, this is somehow expected, due to the fact that a Gaussian distribution gives extremely low probability outside of the $\pm 3\ \sigma$ range; therefore, despite the Poisson prior discouraging larger models, a two–dipole model with small intensities has higher prior probability than a single–dipole model with strong dipole moment; since the likelihood of the two configurations is the same, the posterior peaks on the two–dipole model.

	Δ_d	Δ_c
$\sigma_q = 1$	0.20 ± 0.71	(1.96 ± 3.65) mm
$\sigma_q = 5$	-0.20 ± 0.40	(2.53 ± 9.71) mm
$\sigma_q = 10$	-0.26 ± 0.44	(1.41 ± 3.99) mm

Table 2. Discrepancy measures for the number of dipoles (left) and their location (right) averaged over 100 runs for different values of the parameter σ_q.

5.2. Experiment 2: Variance Comparison

In order to investigate the differences between the semi–analytic approach and the full SMC presented in [26] we produced a dataset containing only a single time point; the data are generated by two sources, one deeper than the other. Dipole strenghts were both set to 1 while their directions are along one of the coordinate axes. White Gaussian noise was added, with standard deviation set to 5% of the peak of the noise-free signal, corresponding to a SNR similar to that of evoked responses.

We do 200 runs of both the algorithms, the semi–analytic SMC and the full SMC, with the same data as input. We set the number of particles I to 100, we use a Gaussian prior for the dipole moment with zero mean and covariance matrix $\Gamma_{q_0} = \mathbf{I}$ and a Gaussian likelihood with zero mean and covariance matrix $\Gamma_e = \sigma_e^2 \mathbf{I}$ where σ_e is set to the true value, i.e. the value actually used to simulate the noise.

In order to quantify the variance between different runs we calculate the sample standard deviation of the intensity measure for the source location in the following way. For each run l, we compute the quantity

$$\mathbb{P}_l(c|y) \simeq \sum_{i=1}^{I} W^i \sum_{k=1}^{D^i} \delta(c, C^{(k),i}). \tag{40}$$

that is an approximation to the intensity measure, differing from equation (37) because here there is no conditioning on the estimated number of dipoles; therefore, all particles

contribute to the calculation of this quantity. Then we compute the sample standard deviation of $\mathbb{P}_l(c|y)$ over runs. In Figure 3 we compare the standard deviations produced by the two algorithms, the full SMC (dark blue bar) and the semi–analytic SMC (red bar), on the subset of points where such standard deviation is higher than $5 \cdot 10^{-3}$. The values of the standard deviation of the full SMC are sorted in descending order, then the standard deviations of the semi–analytic SMC on the corresponding brain grid points are superimposed: the semi–analytic SMC clearly produces lower–variance approximations of the posterior distribution. In Figure 4 we provide the complementary information of what grid points are affected by higher variance: as expected, these points concentrate around the true sources (yellow diamonds), where the posterior probability is higher. The Figure also demonstrates that the points involved by the semi–analytic SMC are fewer. Finally, both algorithms produce higher variance in correspondence of the deeper source.

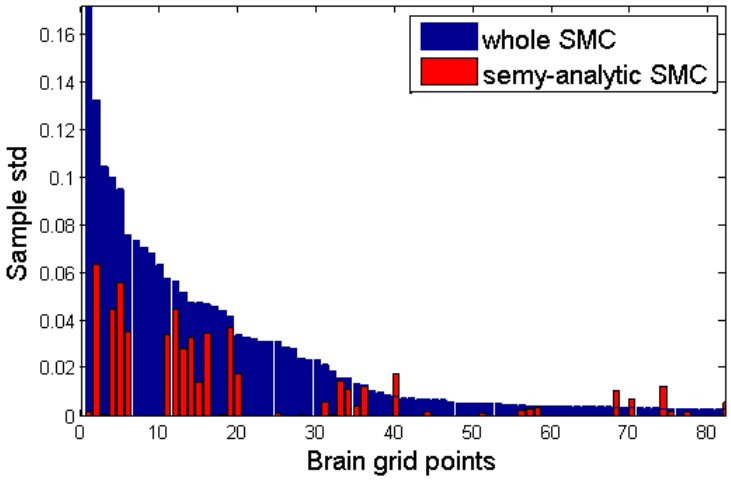

Figure 3. Sample standard deviation over the brain grid point for the two algorithms.

5.3. Experiment 3: Dependence of the Execution–Time on the Length of the Time Window.

In this section we study how the run–time of the algorithm depends on the length of the time window given in input. We do this by means of direct numerical simulation, because the computational cost of the algorithm is itself a Random Variable, and can change considerably depending on the number of sources to be estimated, that, in turn, also tunes the adaptively chosen number of iterations. In addition, the main practical advantage of the proposed method, against the full SMC, consists in opening the possibility to estimate dipoles from a whole time window, maintaining, as we are going to show, the same computational cost needed for a single time point.

We proceed as follows. We consider one of the data set described in the previous section in the case of two correlated dipoles and we extract from it 5 time windows of

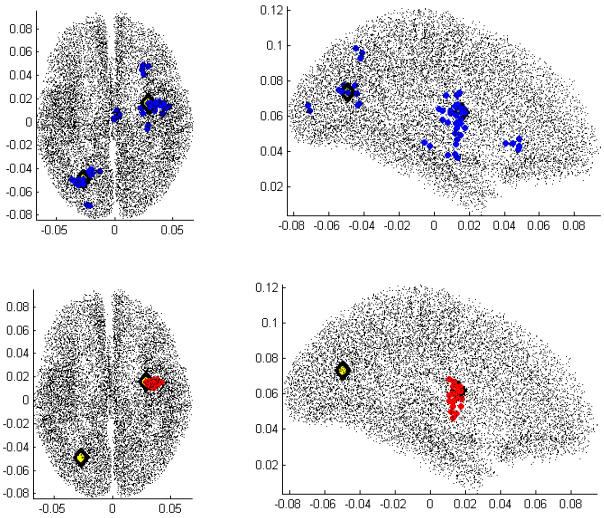

Figure 4. Sample standard deviation on the brain. In each figure we plot the true location of sources (yellow diamond), and the brain grid points whose standard deviation is over a threshold equal to $5 \cdot 10^{-3}$ (blue points for the full SMC, first raw, and red points for the semi–analytic SMC, second raw).

different lengths, namely of length 1, 5, 10, 20, 30. All the time–series are centered in the middle point of the original dataset ($t = 15$), to be sure that the true number of dipoles is the same in all the time windows. Coherently with what we have done in the previous Section, the time–series are analyzed setting $I = 1000$, $\sigma_{q_0} = 1$ and σ_e equal to the standard deviation of the noise. In all the cases the number of dipoles and their locations are estimated correctly and the amount of time spent by the algorithm is approximately the same, as Table 3 shows.

Window size	Time	Iteration
1	54.01 min	159
5	56.97 min	162
10	50.22 min	150
20	46.68 min	147
30	50.19 min	151

Table 3. Run–time in minutes, and number of iterations made when different time windows are given in input. The number of particles I is set equal to 1000.

In order to understand this result observe that the vast majority of computational effort is spent in the evaluation of the marginal log-likelihood, essential to calculate the particle weights. If the assumptions largely described in the previous Sections hold, when a time–window is given in input the total marginal likelihood is the product of

the likelihood at different time points; then, given a particle R_n^i

$$\log(\pi(\mathbf{y}|R_n^i)) = \sum_{t=1}^{N_t} \log(\pi(y_t|R_n^i)). \tag{41}$$

Moreover, $\pi(y_t|R_n^i)$ is a zero–mean Gaussian distribution, whose covariance matrix $\Gamma(R_n^i) = \sigma_{q_0}^2 G(R_n^i)G(R_n^i)^T + \sigma_e^2 \mathbf{I}_{N_s}$ is the same at all time points. Therefore

$$\log(\pi(\mathbf{y}|R_n^i)) = -\frac{N_t}{2}\log\left(\det(\Gamma(R_n^i))\right) - \frac{1}{2}\sum_{t=1}^{N_t}\log\left(y_t^T\Gamma(R_n^i)^{-1}y_t\right) + c. \tag{42}$$

where $c = -\frac{N_s\,N_t}{2}\,\log(2\pi)$ is an additive constant that is common to all particles and therefore does not have to be actually calculated, because it disappears during the normalization.

Here, the most time–consuming operations are the computation of the determinant $\det(\Gamma(R_n^i))$ and of the inverse matrix $\Gamma(R_n^i)^{-1}$, of size $N_s \times N_s$; both operations need to be done only once per particle, and do not depend on the length of the time window. The only calculation that has to be repeated for all the time–points is the matrix-vector product $y_t^T\Gamma(R_n^i)^{-1}y_t$, which is negligible in terms of computational time.

Observe that this result is strictly due to the model structure, i.e., to the assumption of independence between different time points and stationarity of the noise and prior covariances. Indeed, removing the assumption of independence, $\Gamma_{\mathbf{q}}$ and/or $\Gamma_{\mathbf{e}}$ would no longer be block–diagonal; as a consequence the factorization (41) would not hold and we would be forced to compute the high–dimensional Gaussian distribution $\pi(\mathbf{y}|R_n^i)$. In turn, this would require the computation of the determinant and the inversion of a large matrix, of size $(N_s \cdot N_t) \times (N_s \cdot N_t)$. In this case, the computational cost would therefore depend on the length of the time–window N_t and may become potentially unbearable as N_t increases.

6. Application to Experimental Data

We demonstrate the semi–analytic SMC on an experimental dataset recorded during stimulation of the median nerve (Somatosensory Evoked Fields, SEF). The somatosensory response to this type of stimuli is indeed relatively well understood and is often used as a reference for validation on real data. We use the very same dataset used in [26] and, as a further validation, we also report here the source estimates obtained with the full SMC, and with two largely used inverse methods, dynamic Statistical Parametric Mapping (dSPM [2]) and sLORETA [19]. Importantly, these three additional methods take in input a single time point rather than a time–series; here we compare the estimates obtained by the semi–analytic SMC using a time window, with those obtained by these methods at the signal peak in the same window. In addition, the last two methods are not based on a dipolar source model, but on a distributed source

model instead: in particular, dSPM computes first the Tichonov solution of the inverse problem, and then calculates a normalized version that turns out to be t-distributed under the null hypothesis of no activation. SLORETA has a similar approach, but the resulting quantity has a different distribution. Therefore, the comparison has to be considered as a qualitative comparison rather than a quantitative one.

We refer to [26] for a detailed description of the data and of the pre–processing steps. Here we recall that the expected neural response to stimulation of the median nerve [15] comprises a first activation in the primary somatosensory cortex around 25 ms after the stimulus, in the hemisphere contralateral to the stimulation, a later activation of parietal sources around 50 ms after the stimulus, and finally possibly frontal sources around 100 ms.

We applied the semi–analytic SMC with 1,000 particles. We used a diagonal covariance matrix in the likelihood function, corresponding to assuming spatially uncorrelated noise; the standard deviation was estimated from the pre–stimulus interval, by taking the maximum value among the standard deviations of individual channels. The standard deviation of the prior for the dipole moment was set to 20 nAm. We analyzed the three time windows $17.5 - 35$ ms, $37.5 - 75$ ms and $115 - 130$ ms.

In Figure 5 we show the estimated sources, super–imposed on an inflated representation of the cortical surface: light grey represents the gyri, dark grey the sulci, and color is used to represent either the posterior probability (for the two SMCs) or the estimated activity (for dSPM and SLORETA). We remark that such visualization might be misleading, inasmuch the inflation process tends to move apart closeby regions; hence, multiple blobs in the same area are often the consequence of nearby probable/active volume. We also recall that dSPM and SLORETA tend to provide widespread maps for relatively strong sources, and less diffused maps for relatively weak sources, while the two SMC do the opposite, because when a source is strong the posterior probability is highly peaked and viceversa. In light of this, the results of the semi–analytic SMC are in full agreement with those obtained by the full SMC, and seem to be richer than those obtained by dSPM and SLORETA. Indeed, in the first row the localization of the primary somatosensory cortex is the same with all methods. In the second time window/peak, the methods agree on the localization of the source in the right hemisphere; the two SMC also estimate a source in the left hemisphere, which seems to be in accordance, for location and latency, with the literature on SEF responses [15]. Similar considerations apply for the third time window/peak, where the primary somatosensory area is again active, and the two SMC localize an additional source in the frontal region, confirmed by the literature. In the two latter time windows, the semi–analytic SMC also finds, respectively, one and two additional sources in the central region of the brain; however, as they are characterized by a lower probability and intensity, we are not showing them here. The temporal waveforms of the sources estimated by the semi–analytic SMC are shown in Figure 6.

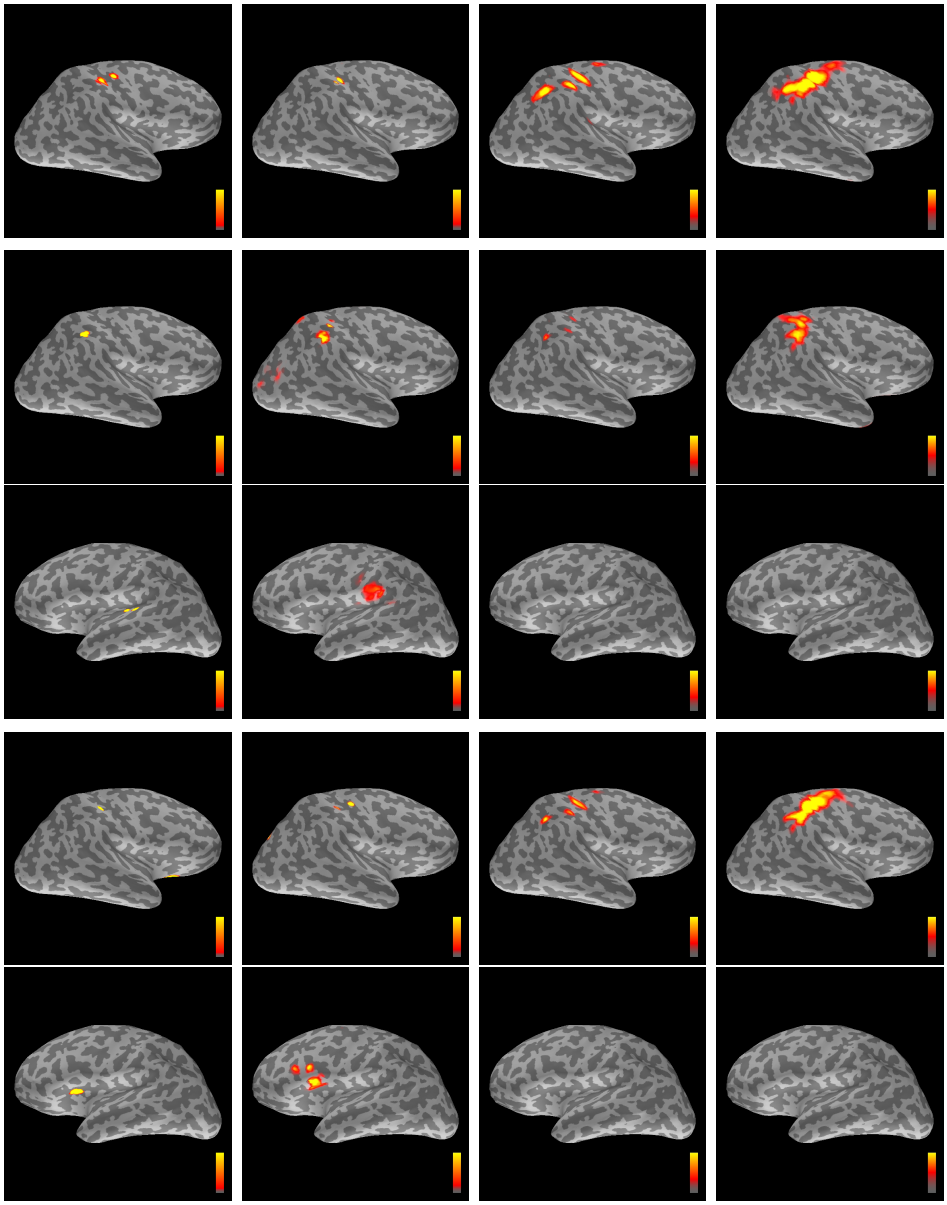

Figure 5. Source estimates computed with the semi–analytic SMC (first column), the full SMC (second column), dSPM (third column) and SLORETA (fourth column).

7. Discussion

In this paper we have described how to use a recent class of Monte Carlo algorithms, called SMC samplers, for solving Bayesian inverse problems described by a semi–linear structure, i.e. when the data depend linearly on a subset of the unknowns and non–linearly on the remaining ones.

First we have shown that, under Gaussian assumptions for the likelihood and for the prior over the linear variables, it is possible to compute a closed form of the marginal likelihood for the non–linear variables and for the conditional posterior distribution for

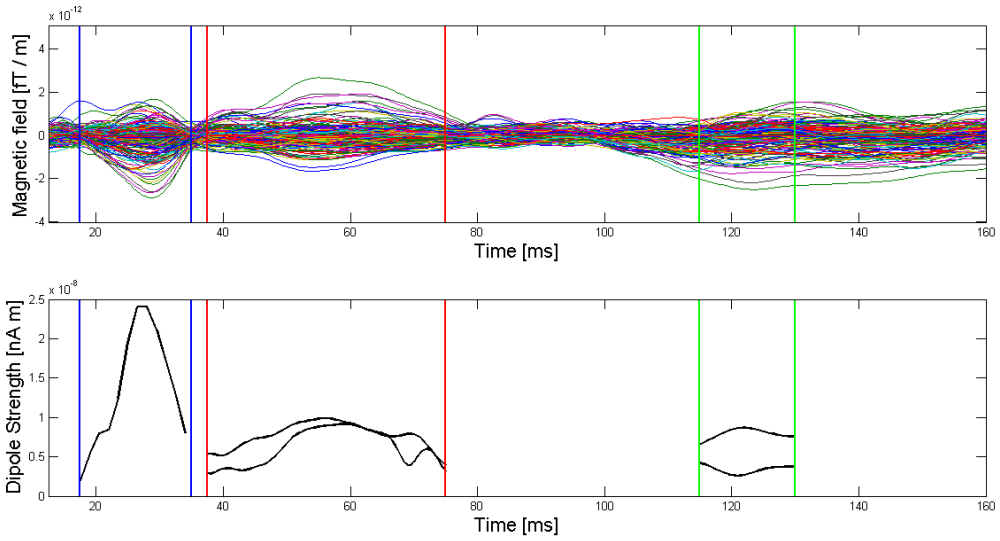

Figure 6. Top panel: the MEG data, and the three temporal windows selected for the analysis. Bottom panel: estimated source time courses for the sources shown in Figure 5.

the linear ones. Therefore, the SMC sampler needs only to be applied to approximate the marginal posterior for the non–linear variables, with the obvious advantage that part of the solution is computed analytically. Second, we have observed that the sequence of distributions naturally chosen for the semi–analytic SMC does not coincide with the sequence of the marginal distributions one would use in the full SMC. Instead, the distributions used in the first step of the semy–analytic SMC can be interpreted as the marginals of the posterior densities of a Bayesian model in which both the noise standard deviation and the prior for the linear and the non–linear variables change with the iterations. Therefore, the full SMC and the semi–analytic SMC reach the same target distribution following different paths. From a theoretical perspective, it remains interesting to extend the class of models to which we can apply this semi–analytic approach beyond just the class of Gaussian models. For instance, one may introduce a hierarchical structure and choose a suitable hyperprior for the parameters that are fixed a priori in our current approach, like the noise standard deviation and the variance of the prior for the linear variables; for example, choosing a gamma–inverse hyperprior would lead to a student-t distribution.

Then we have applied the semi–analytic method to the inverse problem in MEG, where one wants to reconstruct the brain activity from the recorded magnetic field. Here we have introduced several hypotheses about the model structure. First of all we have used a multi–dipole model, in which data depend linearly on the moments of the current dipoles, but not on their number and locations. In this context our approach extends the work of [26], where a full SMC was used to estimate multiple dipoles from a single spatial distribution of the magnetic field: here, by exploiting the linearity with respect to the

dipole moments, we can use the semi–analytic SMC to estimate sources from a whole time–series, under the assumption that the number of dipoles and their locations do not change in time. Such combined use of data at different time points is advantageous at least for two reasons. On one hand, a time–series will contain more information about the source than a single time point, and should therefore enable more accurate localization of the dipoles; in this respect, our approach is prefereable to the use of several independent samplers, each one applied to a different time point. On the other hand, the computational cost of the proposed algorithm is dominated by calculations that do not depend on the length of the time–window, thanks to the additional assumption of independence between different time points. Alternative choices may include to model the linear variables as a Hidden Markov Model and apply Kalman filtering/smoothing for their estimation, like in [9].

We validated our method with different simulated experiments. First of all, we have shown that the semi–analytic method produces lower–variance approximations of the marginal distributions for the source locations, compared to those produced by a full SMC sampler. This means that, the number of particles being equal, the approximations obtained by different runs of the semi–analytic SMC are more similar to each other than those obtained by different runs of the full SMC. This was expected, as a natural consequence of the fact that we are sampling many fewer variables.

Then we have tested the behavior of the proposed algorithm with time–series generated by source configurations containing between 2 and 4 dipoles, with different levels of temporal correlation. The results show that our approach is able to estimate with high accuracy correlated as well as uncorrelated sources. Indeed, in all conditions the localization error remains of the order of few millimeters. An indirect comparison with [26] suggests that we have improved in terms of localization accuracy, as our localization error obtained from noisy data is lower than that obtained with noise–free data by the full SMC, particularly for the more numerous configurations. We have also investigated the behaviour of the method with respect to a mis–specification of the prior. We have shown that a mis–specification of the standard deviation for the dipole moment leads to a worsening of the performances. Namely a too small value may lead to replacing a single true dipole with two estimated ones, while a too large value may lead to missing a weak source. This suggests that the Gaussian distribution with fixed standard deviation might be a bit too restrictive: possible future work may include adaptive estimation of this parameter, or the use of a different prior distribution, as suggested earlier in this Section. As a last numerical experiment, we have used simulations to show that the computational time of the algorithm does not depend on the length of the time window given in input.

Finally, we have analyzed an experimental data set recorded during somatosensory stimulation. Here, we have observed that the estimates produced by the semi–analytic SMC are in full agreement with those obtained by the full SMC, and provide in addition the time courses of the sources. The spatial maps produced by the semi–analytic SMC are slightly more focal, reasonably due to the fact that a time window carries

more information about the source location than a single time point. On the other hand, the new method also localizes few additional sources in the middle of the brain, although with lower probability and intensity, that seem not to be due to physiological activity. Possible explanations of this drawback include modeling errors, such as non perfectly stationary source locations, or the presence of spatial correlation in the noise components.

Future research will be devoted to better asses the performance of the proposed method in real scenarios. In addition, it would be helpful to decrease the computational cost by parallelizing the code with GPU programming.

References

[1] C. Campi, A. Pascarella, A. Sorrentino, and M. Piana. A Rao-Blackwellized particle filter for magnetoencephalography. *Inverse Problems*, 24:025023, 2008.

[2] A. Dale, A.K. Liu, B.R. Fischl, R.L. Buckner, J.W. Belliveau, J.D. Lewine, and E. Halgren. Dynamic statistical parametric mapping: Combining fmri and meg for high-resolution imaging of cortical activity. *Neuron*, 26:55–67, 2000.

[3] G. Dassios, A.S. Fokas, and F. Kariotou. On the non-uniqueness of the inverse MEG problem. *Inverse Problems*, 21:L1–L5, 2005.

[4] P. Del Moral, A. Doucet, and A. Jasra. Sequential Monte Carlo samplers. *Journal of the Royal Statistical Society B*, 68:411–436, 2006.

[5] P. Del Moral, A. Doucet, and A. Jasra. An adaptive sequential Monte Carlo method for approximate Bayesian computation. *Statistics and Computing*, 22:1009–1020, 2012.

[6] A. Doucet, S. Godsill, and C. Andrieu. On sequential monte carlo sampling methods for bayesian filtering. *Statistics and Computing*, 10:197–208, 2000.

[7] A. Doucet and A.M. Johansen. A tutorial on particle filtering and smoothing: Fifteen years later. In *The Oxford Handbook of Nonlinear Filtering*. Oxford University Press, 2011.

[8] A.S. Fokas, Y. Kurylev, and V. Marinakis. The unique determination of neuronal currents in the brain via magnetoencephalography. *Inverse Problems*, 20:1067–1082, 2004.

[9] F. Giraud, P. Minvielle, and P. Del Moral. Advanced interacting sequential Monte Carlo sampling for inverse scattering. *Inverse Problems*, 29:095014, 2013.

[10] P.J. Green. Reversible jump Markov Chain Monte Carlo computation and Bayesian model determination. *Biometrika*, 82:711–732, 1995.

[11] M. Hämäläinen, R. Hari, J. Knuutila, and O.V. Lounasmaa. Magnetoencephalography: theory, instrumentation and applications to non-invasive studies of the working human brain. *Reviews of Modern Physics*, 65:413–498, 1993.

[12] S.C. Jun, J.S. George, J. Paré-Blagoev, S.M. Plis, D.M. Ranken, D.M. Schmidt, and C.C. Wood. Spatiotemporal bayesian inference dipole analysis for MEG neuroimaging data. *NeuroImage*, 28:84–98, 2005.

[13] S.C. Jun, J.S. George, S.M. Plis, D.M. Ranken, D.M. Schmidt, and C.C. Wood. Improving source detection and separation in a spatiotemporal bayesian inference dipole analysis. *Physics in Medicine and Biology*, 51:2395–2414, 2006.

[14] S. Kirkpatrick, C.D. Gelatt, and M.P. Vecchi. Optimization by simulated annealing. *Science*, 220:671–680, 1983.

[15] F. Mauguiere, I. Merlet, N. Forss, S. Vanni, V. Jousmaki, P. Adeleine, and R. Hari. Activation of a distributed somatosensory cortical network in the human brain. A dipole modelling study of magnetic fields evoked by median nerve stimulation. part I: location and activation timing of SEF sources. *Electroencephalography and Clinical Neurophysiology*, 104:281–289, 1997.

[16] J.C. Mosher and R.M. Leahy. Source localization using Recursively Applied and Projected (RAP) MUSIC. *IEEE Transactions on Signal Processing*, 47:332–340, 1999.

[17] J.C. Mosher, P.S. Lewis, and R.M. Leahy. Multiple dipole modeling and localization from spatio-temporal MEG data. *IEEE Transactions on Biomedical Engineering*, 39:541–557, 1992.

[18] C.F.H. Nam, J.A.D. Aston, and A.M. Johansen. Quantifying the uncertainty in change points. *Journal of Time Series Analysis*, 33:807–823, 2012.

[19] R.M. Pascual-Marqui. Standardize low resolution electromagnetic tomography (sLORETA: technical details. *Methods and Findings in Experimental and Clinical Pharmacology*, 24:5–12, 2002.

[20] S. Sarkka, A. Vehtari, and J. Lampinen. Rao-blackwellized particle filter for multiple target tracking. *Information Fusion*, 8:2–15, 2007.

[21] J. Sarvas. Basic mathematical and electromagnetic concepts of the biomagnetic inverse problem. *Phys. Med. Biol.*, 32:11–22, 1987.

[22] D. Schuhmacher, B.T. Vo, and B.N. Vo. A consistent metric for performance evaluation of multi-object filters. *IEEE Transactions on Signal Processing*, 56:3447–3457, 2008.

[23] K. Sekihara, S.S. Nagarajan, D. Poeppel, A. Marantz, and Y. Miyashita. Application of an meg eigenspace beamformer to reconstructing spatio-temporal activities of neural sources. *Human Brain Mapping*, 15:199–215, 2002.

[24] E. Somersalo and J.P. Kaipio. *Statistical and computational inverse problems*. Springer Verlag, 2004.

[25] A. Sorrentino, A.M. Johansen, J.A.D. Aston, T.E. Nichols, and W.S. Kendall. Dynamic filtering of static dipoles in Magnetoencephalography. *Annals of Applied Statistics*, 7:955–988, 2013.

[26] A. Sorrentino, G. Luria, and R. Aramini. Bayesian multi-dipole modeling of a single topography in meg by adaptive sequential monte-carlo samplers. *Inverse Problems*, 30:045010, 2014.

[27] A. Tarantola and B. Valette. Inverse problems = quest for information. *Journal of Geophysics*, 50:159–170, 1982.

[28] B.D. Van Veen, W. van Drongelen, M. Yuchtman, and A. Suzuki. Localization of brain electrical activity via linearly constrained minimum variance spatial filtering. *IEEE Transactions on Biomedical Engineering*, 44:867–880, 1997.

[29] M. Vihola. Rao-blackwellised particle filtering in random set multitarget tracking. *IEEE Transactions on Aerospace and Electronic Systems*, 43:689–705, 2007.

[30] J. Wan and N. Zabaras. A Bayesian approach to multiscale inverse problems using the sequential Monte Carlo method. *Inverse Problems*, 27, 2011.

[31] Y. Zhou, A.M.Johansen, and J.A.D. Aston. Towards automatic model comparison, an adaptive sequential monte carlo approach. *arXiv*, stat.ME:1303:3123, 2013.